Oscillatory convective structures and solutal jets originated from discrete distributions of droplets in organic alloys with a miscibility gap

Marcello Lappa[a)]
Microgravity Advanced Research and Support Center, Via Gianturco 31, 80146 Napoli, Italy

(Received 7 September 2005; accepted 8 March 2006; published online 17 April 2006)

The pattern formation process driven by N droplets out of thermodynamic equilibrium, uniformly distributed on the bottom of a container filled with a partially miscible organic liquid, is investigated for different values of N by means of a multiprocessor solution of the Navier-Stokes equations. The considered system is intended to model the typical phenomena occurring during the thermal processing of liquid-liquid systems exhibiting a miscibility gap (the so-called "immiscible alloys"). These alloys undergo sedimentation of the separated heavier phase to the bottom of the container under normal gravity conditions. Droplets in nonequilibrium conditions are responsible for the occurrence of still poorly known fluid-dynamic instabilities. In the present analysis we provide a clear and quite exhaustive picture of the different stages of evolution of fluid motion inside the container. The distribution of solute is found to depend on the complex multicellular structure of the convective field and on associated "pluming phenomena." Significant adjustments in the pattern take place as time passes. The structure of the velocity field and the number of rising solutal plumes exhibit sensitivity to the number of droplets and to the possible presence of surface Marangoni effects. New classes of possible instability mechanisms (pulsating, traveling, erratic) are identified and described. The investigation provides "local" details as well as general rules and trends about the macroscopic evolution (i.e., "ensemble behaviors") of the system. © *2006 American Institute of Physics*. [DOI: 10.1063/1.2192531]

I. INTRODUCTION

The properties of many types of materials are linked to their crystalline and chemical structure; a relevant example is given by the mechanical strength and corrosion resistance of many metallic composites; these features are determined by the internal structure, which develops as the alloy solidifies from its molten state. Research in this area is primarily concerned with advancing the understanding of the related processing so that the structure and, ultimately, properties of the alloy, can be controlled as the materials are originally formed. Understanding how the method used to produce, or process, a material affects its structure and its properties will help us to make improved materials for many purposes.

Within this context, of particular interest is the case of the so-called organic and inorganic "immiscible alloys" (sulfides and silicates systems, glasses, many metallic composites used as superconductors, magnetic materials, and high-performance electrical contacts).

These special alloys exhibit two immiscible liquid phases within a certain temperature range. In particular, for a monotectic system a homogeneous solution exists only at temperatures above the so-called critical temperature T_c. When $T<T_c$ the melt starts to decompose into two liquid phases. Above the so-called critical temperature T_c both components are completely miscible in the liquid state. Below this temperature two immiscible liquids of different composition and density coexist (the so-called "majority" and "minority" phases).

In the Earth's gravitational field, however, the usual differences in density cause rapid spatial separation of the alloy components through sedimentation or flotation. This prevents homogeneous distribution of particles in the matrix using simple and inexpensive casting processes (Ratke,[1] Wu *et al.*[2]).

Superimposed on this is the fact that during the solidification process, the melt is subject to temperature gradients. In a gravity field, they lead in most cases to buoyancy driven convective flows, and regardless of the presence of gravity (i.e., also under microgravity conditions), they can produce Marangoni stresses at the interface between the two liquids.

These stresses have been found to be directly or indirectly responsible for several additional complex and intriguing phenomena. In microgravity conditions they act as the driving force for the so-called "Marangoni migration": due to the surface Marangoni stress distribution induced by thermal effects, free liquid drops surrounded by an immiscible liquid migrate toward the hot region (see, e.g., Bassano,[3] Lappa,[4] and Esmaeeli[5]). On the ground the presence of thermal Marangoni surface stresses can be the source of fascinating fluid-dynamic instabilities driven by the direct opposition of thermal to solutal (dissolution) effects.[6,7]

Even if, as explained before, the phases behave as immiscible liquids when they are formed, droplets, formed in some regions by cooling of the considered alloy, can move, owing to the aforementioned gravitational sedimentation, to regions with different temperatures, e.g., toward the bottom of the container that is typically colder than the top (the system is usually cooled from below to avoid the onset of

[a)]Fax: +39-81-6042100. Electronic mail: lappa@marscenter.it

massive thermal buoyancy convection). Since the phases, on the basis of the phase diagram, have different equilibrium concentrations at different temperatures, a droplet that is in equilibrium (i.e., immiscible) with the surrounding liquid in a certain region at a certain temperature will be no longer in such a stable condition if it rapidly moves to another zone with a different temperature. Therein, in fact, it will tend to return to an equilibrium exchanging mass with the surrounding phase and leading to the onset of solutal convection.

Owing to this behavior, the interaction between liquid drops and the surrounding fluid becomes very complex. It is manifested by a fluid motion brought about by different coexisting mechanisms: Marangoni convection, generated by the interfacial stresses due to temperature gradients along the drop surface (thermocapillary convection) and gravitational convection driven by the volumetric buoyancy forces caused by thermally and/or solutally generated density variations in the bulk of the fluid. As outlined above, the delicate interplay among these effects can lead to the onset of oscillatory phenomena.

These instabilities represent an additional aspect of the problem that should be taken into account in addition to the aforementioned migration and sedimentation mechanisms pertaining to the droplets. Along these lines, some interesting experimental and numerical results have been recently obtained by Lappa *et al.*[6,7] The case of a single dissolving droplet in nonequilibrium conditions was considered. The onset of oscillatory convection was investigated for different possible initial volumes of the droplet. These results were refined by Lappa and Piccolo,[8] who reported a variety of possible scenarios as a function of the applied temperature gradient. Among other things, these studies clearly highlighted that, beyond technological aspects, the considered single-drop configuration tends to behave as an intriguing pattern-forming dynamical system.

Due to such a feature, in addition to its technological and industrial significance, it is clear that the problem under investigation also exhibits a theoretical kinship with the complex of problems that come under the heading "route to chaos." Hence, it can be also regarded as an interesting and relevant subject of investigation within the framework of fundamental studies focused on the possible bifurcations of complex systems (see also, e.g., Refs. 9–11).

The aim of the present paper is to extend the earlier results,[6–8] to the more realistic situation in which a relatively large number of droplets are uniformly distributed on the bottom of the container (i.e., a discrete layer of N drops for different values of N).

The convective structures originated from the different droplets can interact in unexpected ways. Therefore, "ensemble behaviors" with many interacting droplets, must be regarded as an important aspect of the problem. Due to their geometric complexity, such configurations have not been studied in great detail. They are still a challenging task for numerical simulation. Nevertheless, numerical simulations are of fundamental importance within the context of these studies. From an experimental point of view, in fact, for $N > 1$, the pattern (interferometric fringes) becomes so complex that a coherent reconstruction of the underlying velocity and concentration distributions is very difficult (often impossible).

TABLE I. Physical properties of the cyclohexane-methanol system.

D ($m^2\ s^{-1}$)	2×10^{-9}
ρ_1 ($kg\ m^{-3}$)	0.782×10^{3}
ρ_2 ($kg\ m^{-3}$)	0.769×10^{3}
ν_1 ($m^2\ s^{-1}$)	1.03×10^{-6}
ν_2 ($m^2\ s^{-1}$)	1.275×10^{-6}
β_{c1} (-)	-4.62×10^{-2}
β_{c2} (-)	4.95×10^{-2}
β_{T1} (K^{-1})	1.14×10^{-3}
β_{T2} (K^{-1})	1.14×10^{-3}
C_{p1} ($J\ kg^{-1}\ K^{-1}$)	2.51×10^{3}
C_{p2} ($J\ kg^{-1}\ K^{-1}$)	1.86×10^{3}
λ_1 ($J\ m^{-1}\ s^{-1}\ K^{-1}$)	2.02×10^{-1}
λ_2 ($J\ m^{-1}\ s^{-1}\ K^{-1}$)	1.25×10^{-1}
σ (dyne m^{-1}):	
at 23 °C	374
at 29 °C	253
σ_T (dyne $m^{-1}\ K^{-1}$)	17.42
T_c (K)	318

The present contribution appears as the first attempt to analyze these (fluid-dynamic) global behaviors focusing on both microphysical (fluid motion around the droplets) and macrophysical aspects (global behavior of the system). The analysis is carried out through an application of the numerical method used by Lappa.[12] It is briefly described in Sec. III.

II. LIQUIDS, GEOMETRICAL PARAMETERS, AND CONFIGURATION UNDER INVESTIGATION

A. Liquid-liquid system

Unfortunately, immiscible metal alloys are not transparent to visible light and direct visualization of flows and solutal phenomena is not possible. A miscibility gap in the liquid phase, however, is also found in many other different systems: binary mixtures of organic liquids, sulfides and silicates systems, glasses and liquid crystals. Further to the case of metal alloys, many industrial applications and processes are based on miscibility-gap and related phenomena.

According to the major difficulty in investigating liquid metals for their opaqueness, organic liquids are often used as model substances to study these aspects. For instance, methanol and cyclohexane have been selected and investigated both in earth and in space laboratories since they are transparent liquids exhibiting a miscibility gap in the phase diagram. They are used as model liquids for the present analysis as well (see Table I for the related physical properties). Conditions corresponding to the aforementioned lack of equilibrium (induced by the gravitational shift of droplets formed in the bulk by the spontaneous thermodynamic decomposition process, to zones with different temperature) are reproduced here by simply considering initial conditions with droplets of pure methanol surrounded by pure cyclohex-

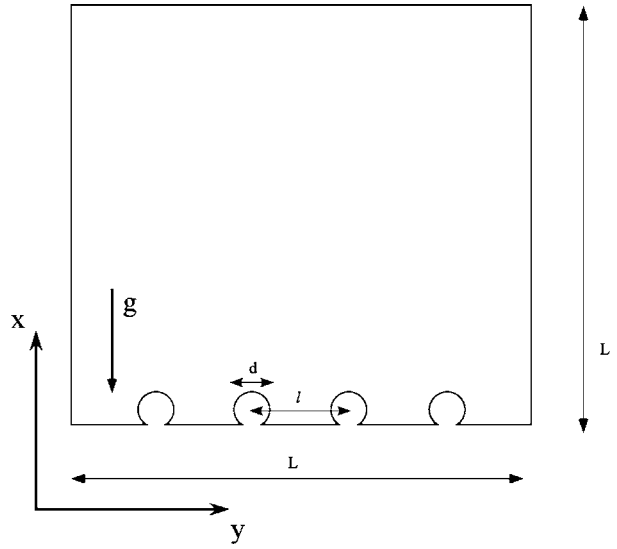

FIG. 1. Sketch of the multidroplet configuration and related geometrical parameters.

ane at a temperature below the critical one (the fluids are miscible in such a condition; see, e.g., Ref. 8). The droplets are supposed to be attached at the tip of the needles used to inject them into the matrix from the bottom of the container.[8] Also, it is supposed that the needles protrude in the text cell only for a few microns (Fig. 1).

B. Geometrical parameters

Since the Bond number is relatively small, Bo $=\Delta\rho\, gR^2/\sigma=3.4\times10^{-2}\ll1$, where σ is the surface tension (e.g., 3.75 dyn/cm at 23 °C), $\Delta\rho$ is the density jump, and $R=d/2$ the droplet radius, the shape of the droplets is assumed to be spherical (i.e., a liquid matrix confined between two parallel and vertical walls with a periodic array of evenly spaced spherical liquid bodies in the interior).

The aspect ratio of the container is defined as $A=L_x/L_y$ ($A=1$ for the present case), x and y being the vertical and the horizontal directions, respectively. Other relevant nondimensional geometrical parameters are the nondimensional diameter of the droplets $A=d/L=0.067$ (L being the characteristic length of the container, $L=3$ cm and $d=2$ mm) and the parameter $\kappa=d/l$ (the ratio of the drop diameter to the distance l between the centers of two consecutive droplets; see Fig. 1). The number of droplets is changed in order to analyze the sensitivity of the overall system to this parameter ($N=4\rightarrow\kappa=0.33$ and $N=5\rightarrow\kappa=0.4$).

The lateral walls are supposed to be adiabatic; no-slip conditions for the velocity are considered along the solid boundaries.

III. THE NUMERICAL METHOD

The model is based on the mass balance equations. The diffusion of the species is governed by the equations (drop =phase $1\rightarrow\phi=1$, matrix=phase $2\rightarrow\phi=0$, where ϕ is the phase variable)

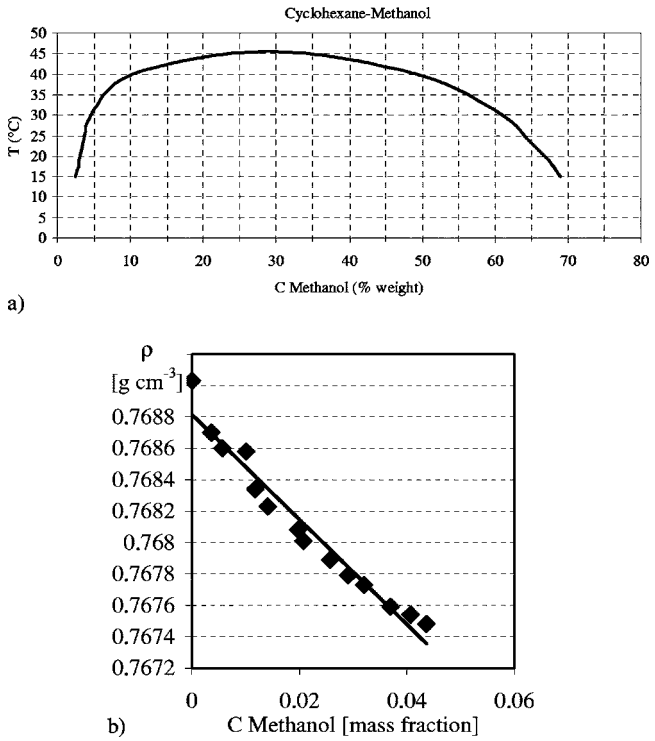

FIG. 2. Phase diagram (a) and density versus methanol concentration (b) for the cyclohexane-methanol system.

$$\frac{\partial C_1}{\partial t}=[-\nabla\cdot(\mathbf{V}C_1)+D\nabla^2C_1],\quad \text{if } \phi=1, \tag{1a}$$

$$\frac{\partial C_2}{\partial t}=[-\nabla\cdot(\mathbf{V}C_2)+D\nabla^2C_2],\quad \text{if } \phi=0, \tag{1b}$$

where $\mathbf{V}$ is the velocity, D is the binary interdiffusion coefficient, and C_1 and C_2 are the concentrations of one of the two components (for the present case it is methanol) in the minority (drop) and majority (matrix) phases, respectively. The initial constant concentrations in the drop and in the matrix are denoted by $C_{1(0)}$ and $C_{2(0)}$, respectively (for the case under investigation: $C_{1(0)}=1$, i.e., a drop of pure methanol and $C_{2(0)}=0$, i.e., matrix of pure cyclohexane).

The behavior of the two phases is coupled through the equilibrium concentration values imposed on the two sides of the interface. These values come from the miscibility law [Fig. 2(a)] according to the local value of the temperature (T) of the interface (for isothermal conditions, of course, the equilibrium values are constant along the interface). At the interface ($0<\phi<1$), the concentrations must satisfy the equilibrium conditions

$$C_1|_i=C_{1(e)}(T), \tag{2}$$

$$C_2|_i=C_{2(e)}(T). \tag{3}$$

Equations (2) and (3) rely on the assumption that equilibrium at the liquid-liquid interface is attained instantaneously (see Perez De Ortizy on the assumption that equilibrium at the liquid-liquid and Sawistowski[13]). Note that, in place of the "sharp" transition from one phase to the other that would

characterize multiple region formulations (in that case the interface separating the bulk phases is a mathematical boundary of zero thickness), here the phase field varies smoothly but rapidly through an interfacial region whose thickness is not zero. This region is defined by the mathematical conditions $|\nabla\phi| \neq 0,\ 0 < \phi < 1$.

Following the usual Boussinesq approximation for incompressible fluids, the physical properties (C_p, μ, λ, etc.) are assumed constant in each of the two phases, except for the density ρ in the generation term in the momentum balance equation, which is assumed to be a linear function of temperature and concentration in each of the two phases, i.e.,

$$\rho_1 = \rho_{1(0)}[1 - \beta_{T1}(T - T_{(0)}) - \beta_{c1}(C_1 - C_{1(0)})], \tag{4a}$$

$$\rho_2 = \rho_{2(0)}[1 - \beta_{T2}(T - T_{(0)}) - \beta_{c2}(C_2 - C_{2(0)})], \tag{4b}$$

$\rho_{1(0)}$ and $\rho_{2(0)}$, being the density of the two phases for $T = T_{(0)}$ (reference temperature) and initial concentration values, respectively; β_{c1} and β_{c2} being the solutal expansion coefficients related to the mutual interpenetration of the phases (1) and (2), β_{T1} and β_{T2}, the thermal expansion coefficients.

In other words, the continuity equation is reduced to the vanishing of the divergence of the velocity field, and variations of the density induced by solutal and/or thermal gradients are ignored in the momentum equation, except insofar as they give rise to a gravitational force. It is well known that this approximation is extremely accurate and makes the mathematics and physics simpler. Thus, the continuity and Navier-Stokes equations read as

$$\nabla \cdot \mathbf{V} = 0, \tag{5}$$

$$\frac{\partial(\rho \mathbf{V})}{\partial t} = -\nabla p - \nabla \cdot [\rho \mathbf{V}\mathbf{V}] + \nabla \cdot [\mu(\nabla \mathbf{V} + \nabla \mathbf{V}^T)] + \mathbf{F}_{\mathrm{Ma}} + \mathbf{F}_g, \tag{6}$$

where p is the pressure,

$$\rho = \rho_{1(0)}\phi + \rho_{2(0)}(1 - \phi), \tag{7a}$$

$$\mu = \mu_1\phi + \mu_2(1 - \phi), \tag{7b}$$

are the density and the dynamic viscosity, respectively; in the last term of Eq. (6),

$$F_g = -\rho g + \rho g[\beta_{C1}(C_1 - C_{1(0)})]\phi + \rho g[\beta_{C2}(C_2 - C_{2(0)})](1 - \phi) + \rho g[\beta_{T1}(T - T_{(0)})]\phi + \rho g[\beta_{T2}(T - T_{(0)})](1 - \phi). \tag{7c}$$

The source terms $\mathbf{F}_{\mathrm{Ma}}$ take into account the other driving force involved in the phenomena under investigation, i.e., the Marangoni effect.

The strategy used herein to account for this force, in fact, is based on the continuum surface force (CSF) and stress (CSS) models (see Lappa[12] for further details).

Thus, the second source term in Eq. (6) reads as

$$F_{\mathrm{Ma}} = \left(\frac{2\sigma}{R}\hat{\mathbf{n}} - \frac{\partial\sigma}{\partial T}(\mathbf{I} - \hat{\mathbf{n}}\hat{\mathbf{n}}) \cdot \nabla T\right)|\nabla\phi|, \tag{8}$$

where I is the identity matrix and $\hat{\mathbf{n}}$ is the unit vector perpendicular to the fluid/fluid interface, $\hat{\mathbf{n}} = -\nabla\phi/|\nabla\phi|$ pointing toward the matrix.

The temperature distribution is governed by the energy equation

$$\frac{\partial \rho\, C_P T}{\partial t} = [-\nabla \cdot (\rho C_P \mathbf{V} T) + \nabla \cdot (\lambda\, \nabla T)], \tag{9}$$

where the thermal conductivity λ and the specific heat C_P are computed as

$$\lambda = \lambda_1\phi + \lambda_2(1 - \phi), \tag{10a}$$

$$C_P = C_{P_1}\phi + C_{P_2}(1 - \phi). \tag{10b}$$

It should be pointed out that both the shape and the size of the droplets are assumed to be fixed in the present work. The numerical method can handle size changes (see, e.g., the rich comparison between experimental and numerical results about droplet radius evolution in time in Lappa *et al.*[7]). The integration of the jump species balance equation at the interface can be used, in fact, to introduce a global relationship for the time derivative of the radius. The tracking of the interface between the phases can be accomplished by the solution of such a special continuity integral equation for the volume of the liquid drop, taking into account the release or absorption of solute through the interface (the liquid drop being assumed to be a sphere of radius R, increasing due to growth or decreasing due to dissolution, and the distribution of the phase-field variable being reinitialized at each instant according to the current value of the radius).

In the present simulations this option of the numerical algorithm has been switched off for the following reasons: On the basis of the results discussed in a previous article,[7] for the same conditions considered in the present work [isothermal conditions or $\partial T/\partial x = O(1\ ^\circ\mathrm{C\ cm^{-1}})$] the radius change over a period of about 100 s is very limited (less than 5% of the initial radius; see, in particular, Figs. 5 and 9 in Lappa *et al.*[7]). This means that R can be considered constant without introducing a significant approximation error. Moreover, such an option (radius computation) of the numerical code, when disabled leads to a significant increase of the time integration step required to guarantee numerical stability of the algorithm and, therefore, to a significant shrinkage of the total time required for the computations.

As a consequence, here the phase variable is not updated, but only used as a marker to distinguish the droplets (it behaves as a static variable used to characterize the system geometry).

Equations (1), (2), (5), (6), and (9) are solved with the SMAC method. This method is not described here for the sake of brevity and since it is well known. For further details see, e.g., Ref. 14. The simulations are two-dimensional; nevertheless, the numerical results can be regarded as a good approximation of the real flow for conditions in which the convective structures and the corresponsing solutal jets are

not allowed to expand along the third direction (e.g., the physical domain confined between close walls along z, i.e., $L_z \cong d$).

A grid refinement study (for a single droplet) has been published in Lappa and Piccolo.[8] It is shown therein that to obtain convergence within 1%, it is necessary at least a grid 400×100 (computational domain 4×1). By extrapolation to the present case of a square domain, a grid 400×400 is needed (at least); accordingly, a mesh 500×500 is used. Owing to the enormous time required for the computations, simulations are carried out within the framework of a parallel multiprocessor technique. The problem is split in two problems: one parabolic and the other elliptic. A parallel algorithm, explicit in time, is utilized to solve the parabolic equations (momentum, temperature, and species equations). A parallel multisplitting kernel is introduced for the solution of the pseudopressure elliptic equation, representing the most time consuming part of the algorithm. A grid-partition strategy is used in the parallel implementations of both the parabolic equations and the multisplitting elliptic kernel. A message passing interface (MPI) is coded for interprocessor communications.[14]

IV. RESULTS

As droplets dissolve in the external matrix, each droplet enriches the surrounding fluid of methanol producing a light concentration-enriched zone around it. The density of the majority phase, in fact, is a decreasing function of the methanol concentration [Fig. 2(b)]. Owing to such a feature, for isothermal conditions (e.g., $T=23\ ^\circ\mathrm{C}$), a rising plume is originated above each droplet.

In the region surrounding the generic droplet, the solute concentration changes continuously from the local equilibrium concentration at the droplet surface to the concentration in the bulk of the solution. The related concentration profile varies with time and is controlled by the balance between diffusion of the solute and the tendency of the fluid to rise, owing to solutal buoyancy effects. If a nonisothermal process is considered (the system is heated from above), the tendency of the fluid to be driven from the hot upper regions toward the bottom cold regions due to surface tension (Marangoni) effects also plays a crucial role in the dynamics mentioned previously. For sufficiently large values of the temperature gradient, it can force the layer of liquid surrounding the drop to move downward, even if it is lighter than the matrix.

In addition to these arguments, one must keep in mind that there is an effect related to the fact that, when many droplets dissolve at a close distance, some mutual influence occurs due to superposition and intersection of the related "enriched zones" and/or due to viscous interaction of convective structures originated from their surfaces (rising currents driven by solutal buoyancy effects, or descending currents driven by thermal Marangoni forces). The coupling between these convective "pluming phenomena" and the overlapping of the enriched zones can make the concentration pattern very complex. The next subsections consider the simultaneous presence of many droplets and the related possible mutual interplay; first the results provided by the simulations are depicted in detail; then, Secs. V and VI present some critical and focused discussions (showing analogies and differences among different conditions), a comparison with other results in the literature, and, finally, some interesting insights into the physics.

A. Isothermal conditions

For isothermal conditions, the flow around each droplet is dominated by solutal buoyancy effects. According to the earlier studies of Lappa *et al.*,[6] it is known that in the case of a single droplet, after an initial transient time, a stable buoyant straight rising jet continuously carrying methanol toward the top of the test cell is created.

The present studies prove that this is not the case when an array of droplets is considered (see the detailed discussion later).

For $N=4$, at the beginning, each droplet is characterized by its own rising solutal plume. In this early phase of the dissolution process, the dynamics of the different droplets can be regarded as independent. Two convective cells are generated around each droplet and then rise attached to the mushroom-shaped head (the cap) of the related solutal jet (hereafter the droplets will be referred to as droplet "i" with $i=1 \rightarrow N$, respectively, starting from the left side of the container). However, after a short initial transient behavior the two central rising jets $i=2$ and $i=3$ tend to be featured by a reduced rising velocity with respect to those at the edges [$i=1$ and $i=4$; see Fig. 3(a)]. In practice, they experience the return flow of the lateral jets and for this reason tend to be retarded.

After 46 s [see Fig. 3(c)], the lateral solutal plumes (1 and 2) merge, giving rise to a single rising current. The same behavior holds for the plumes 3 and 4 since the system exhibits mirror symmetry with respect to the midsection $y=L/2$. For this reason, after an initial stage, the lighter fluid is transported upward by two solutal rising jets only. They are located approximately at $y=L/5$, $y=4L/5$, respectively (instead of the four solutal plumes that characterize the system behavior in the early phase located at $y=iL/5$, $i=1 \rightarrow 4$).

Evolution of the surviving solutal plumes results in a shape that bulges out below $y=L/2$ and necks in above it. This leads to an amphora-like pattern [Fig. 3(d)].

For a further increase of time, two new plumes are originated from the central droplets 2 and 3. As they rise, the related combined solute paths result in a shape that necks below $y=L/2$ and bulges out above it [Fig. 3(f)]. This phenomenon is then followed in time by the generation of two new plumes above the lateral droplets 1 and 4 [Fig. 3(g)].

During these stages of evolution, the droplets seem to "work" in mirror groups of two. Rising solutal jets are initially created above the couple (1, 4), then above the couple (2, 3). Then the couple (1, 4) is again involved in the generation of rising jets, and so on. Therefore a certain degree of periodicity in time can be highlighted with mechanisms exhibiting a somewhat "repetitive" behavior. As time passes, new regimes evolve that exhibit a periodic alternance of central or lateral rising plumes.

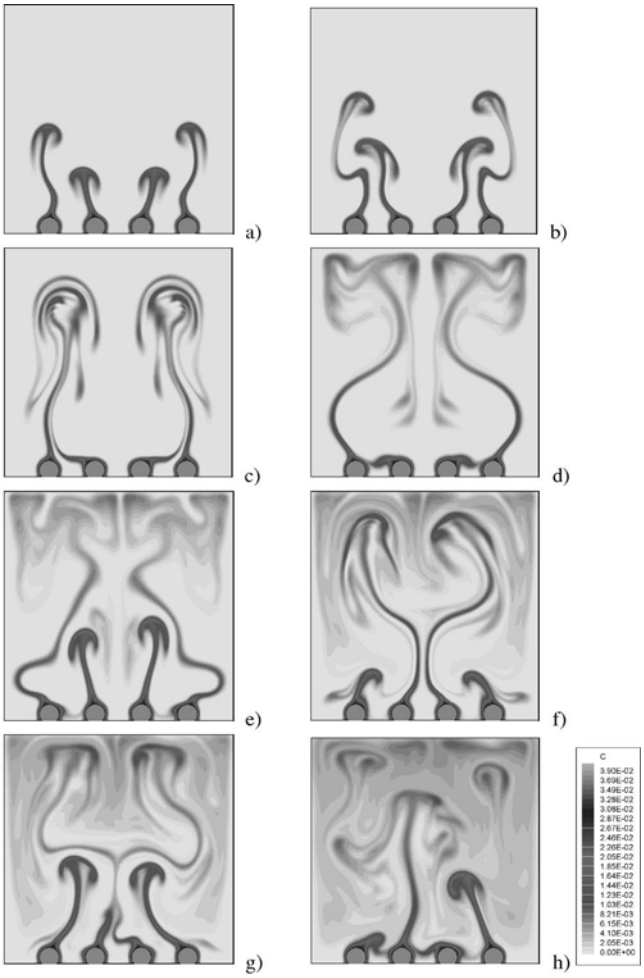

FIG. 3. Computed pattern formation and evolution for the case $N=4$, uniform temperature distribution ($T=23\ ^\circ$C), subsequent snapshots corresponding to (a) $t=35.6$ s, (b) $t=39.2$ s, (c) $t=46.3$ s, (d) $t=57$ s, (e) $t=71.3$ s, (f) $t=82$ s, (g) $t=89.1$ s, (h) $t=114.2$ s.

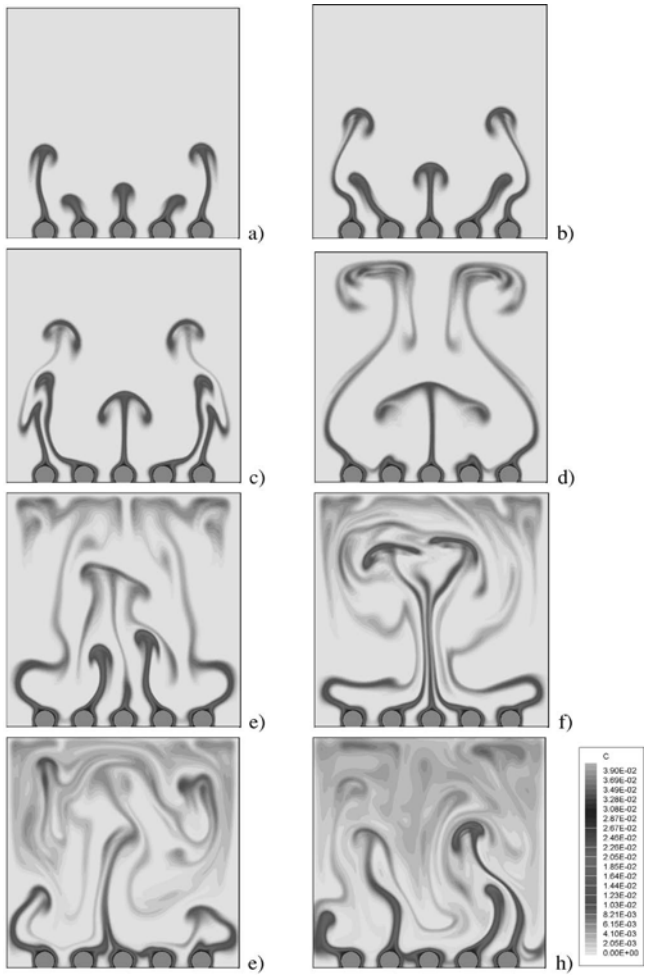

FIG. 4. Computed pattern formation and evolution for the case $N=5$, uniform temperature distribution ($T=23\ ^\circ$C), subsequent snapshots corresponding to (a) $t=35.6$ s, (b) $t=39.2$ s, (c) $t=42.75$ s, (d) $t=53.4$ s, (e) $t=64.1$ s, (f) $t=71.2$ s, (g) $t=81.9$ s, (h) $t=99.75$ s.

These phenomena are also susceptible of an interesting interpretation in terms of relative temporal phase shifts. The phase shift is herein defined as $\pi\,\Delta L/L$, ΔL being the difference between the height (along x) of two plumes at a given instant (this simply means that two plumes having the same height are featured by a zero phase shift, whereas the phase shift is approximately π if two plumes, one extended throughout the container and the other confined to the bottom, are considered).

Periodic convective structures originated from the droplets 1 and 4 do not exhibit phase shift ($\Delta\varphi_{14}=0$). Convective structures originated from the droplets 2 and 3 also do not exhibit phase shift ($\Delta\varphi_{23}=0$). A phase shift $\Delta\varphi=\pi$ occurs between droplets 1 and 2, or 3 and 4 (e.g., a new jet is generated above the second drop when the plume above the first one dies at the top of the cell). This also means that only two values of $\Delta\varphi_{ij}$ are possible (0 or π).

For a further increase of time, however, the spectrum of possible phase shifts becomes more complex. The initial regular pulsating mechanism described above, with a rhythmic alternance of central and lateral couples of rising jets (featured by mirror symmetry with respect to the midsection $y=L/2$) is taken over by a new disordered regime in which the release of plumes seems to be quite erratic or chaotic [see Fig. 3(h)]. In such a regime, the pattern becomes asymmetric and such a symmetry breaking is associated with the presence of a variety of possible phase shifts $\Delta\varphi_{ij}$.

These trends are partially confirmed by the simulations carried out for $N=5$ (Fig. 4).

In such a case, the major stages of the system evolution are quite similar to those discussed before for the case $N=4$: at an early stage, the flow undergoes transition to an oscillatory state featured by a mirror symmetric regular alternance of plumes released by lateral and internal droplets [(1,5) and (2,4), respectively]. In terms of possible phase shift, however, the central drop $i=3$, seems to work independently. The related plume, in fact, is extended along half of the height of the domain when the others have already reached the top of the domain and/or are still confined to a region close to the surface of the droplets [see Fig. 4(d), where plumes 1 and 5 are extended throughout the domain, plumes 2 and 4 are still in very embryonic conditions, and plume 3 affects the lower half of the container]. Accordingly

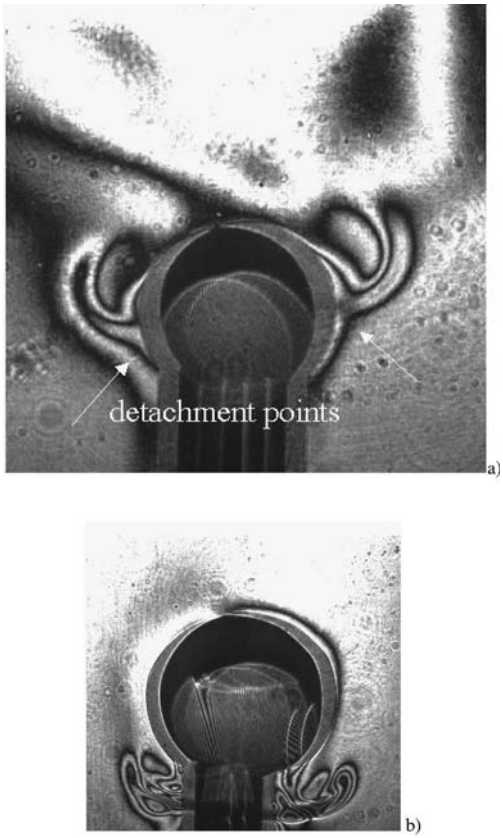

FIG. 5. Experimental evidence of "detachment points" (a) and descending currents (b) in the presence of Marangoni thermal effects [images obtained by means of a Wollaston lateral shearing interferometer (Malacara); see Ref. 8 for further details].

it exhibits a phase shift $\Delta\varphi_{3j} \cong \pi/2$ with respect to the pulsating phenomena pertaining to the other companion droplets.

As time passes, however, as for the case already discussed for the array of four evenly spaced droplets, these regular behaviors are replaced by a quite erratic generation/release of plumes and related possible time shifts [e.g., Fig. 4(h)]; this can be regarded as a significant result, as it highlights the spontaneous tendency of multidroplet configurations to evolve toward final erratic pulsations, regardless of the even or odd number of droplets.

B. Nonisothermal conditions

If a sufficiently large temperature gradient is applied along the drop surface, it is known that even for a single droplet (for a drop with a diameter $d=2$ mm, the critical $\partial T/\partial x$ is about 1.2 °C cm^{-1}), the system can undergo transition to an oscillatory behavior and that such an instability is driven by the opposition of solutal buoyancy to thermal Marangoni stresses.[6–8]

A clear evidence of the counteracting interplay of solutal buoyancy and thermal Marangoni forces is given by the presence along the drop surface of a "detachment point" [Fig. 5(a)]. This point corresponds to the detachment of the layer of liquid transported close to the interface by thermal surface tension forces. Owing to the solutal buoyancy forces that oppose downward motion, the surface layer has not enough momentum to reach the rear of the drop.

When the temperature difference applied to the container is sufficiently high and/or the drop is very close to the bottom wall (the present case), where a thermal boundary layer with steep temperature gradients is present, the detachment point moves to the rear of the droplets [Fig. 5(b)]. For this reason return flow is initiated close to the drop base.

For an array of evenly spaced droplets, the aforementioned return flows give rise to liquid currents that meet each other at about half the distance between consecutive drops. Thus, rising solutal jets are created there [the positions are $y=L/2(N+1)+iL/(N+1)$], whereas the onset of pluming phenomena in the regions above the droplets is prevented. Thus, there is a significant difference with respect to the cases discussed before in which rising jets are originated from the peak of the droplets [i.e., at $y=iL/(N+1)$].

A very complex multicellular structure is created above the discrete distribution of droplets. This convective field undergoes interesting subsequent transitions to different regimes as time passes. It is also worthwhile to stress how, unlike the case of pure buoyancy flow discussed before, the major stages of this spatiotemporal evolution are significantly affected by the value of N ($N=4$ in Fig. 6 and $N=5$ in Fig. 7).

For the case $N=4$, at the beginning five distinct rising convective jets occur [Fig. 6(a)].

After about 30 s [see Fig. 6(b)], the lateral solutal plumes (1 and 2) merge, giving rise to a single rising current. The same behavior holds for the plumes 4 and 5 since the system exhibits mirror symmetry with respect to the midsection, $y=L/2$. For this reason, after an initial stage, the lighter fluid is transported upward by three solutal rising jets only. For a further increase of the time, the simulations show that the system exhibits a pronounced tendency to lose its initial mirror symmetry with respect to the midsection $y=L/2$ [Figs. 6(c) and 6(d)].

The lateral plumes intersect the central one. This is associated with a significant time-dependent mixing of the solute throughout the container. A single vortex expanded throughout the domain is created, in fact, above the droplets [see, e.g., Fig. 6(e)].

This vortex is initially clockwise oriented, but as time passes it is taken over by a counterclockwise new vortex [Figs. 6(g) and 6(h)]. The system then comes back to a clockwise circulation and so on, with a periodic alternance of clockwise and counterclockwise convective structures. Correspondingly, all the rising solutal jets tend to coalesce into a single elongated finger. Such a finger is bent by the action of the aforementioned vortex. It is originated from droplet 2 when the domain is featured by the presence of the clockwise vortex [Figs. 6(e) and 6(f)] and from droplet 3 [Figs. 6(g) and 6(h)] when the system undergoes transition to the counterclockwise one, respectively (the frequency of this phenomenon is given in Table II).

As anticipated, for $N=5$ the roll-pattern formation and evolution are quite different. At the beginning [Fig. 7(a)], six rising plumes appear above the seeds ($i=1\rightarrow6$). For t

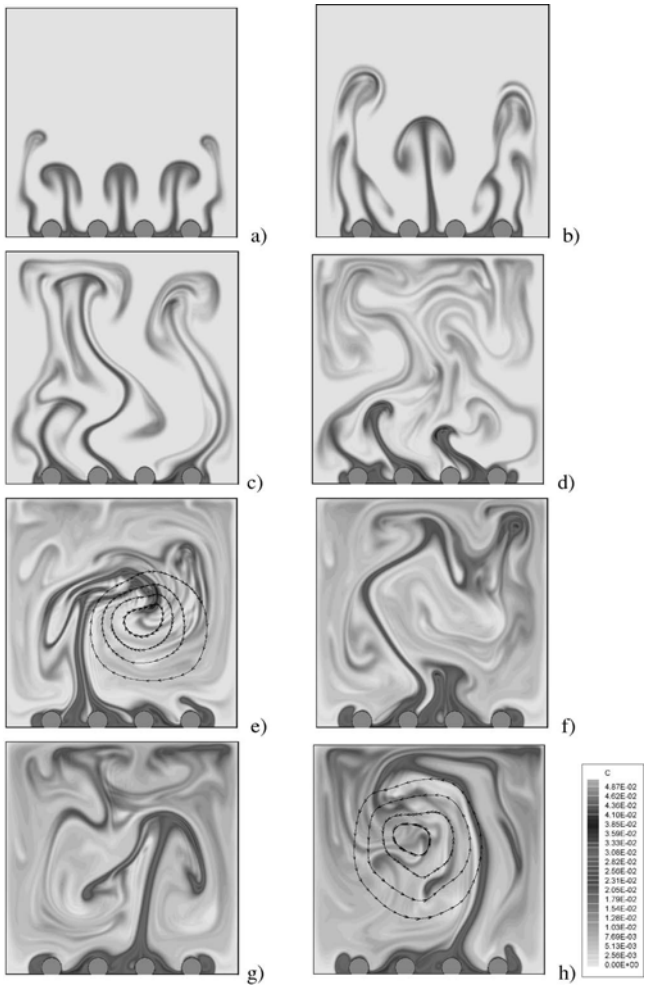

FIG. 6. Computed pattern formation and evolution for the case $N=4$, with $\partial T/\partial x=2\ ^\circ\mathrm{C\ cm^{-1}}$ ($T_{\mathrm{bottom}}=23\ ^\circ\mathrm{C}$, $T_{\mathrm{Top}}=29\ ^\circ\mathrm{C}$), subsequent snapshots corresponding to (a) $t=26.9$ s, (b) $t=32.9$ s, (c) $t=44.9$ s, (d) $t=55.3$ s, (e) $t=65$ s, (f) $t=73.1$ s, (g) $t=78.6$ s, (h) $t=84.1$ s.

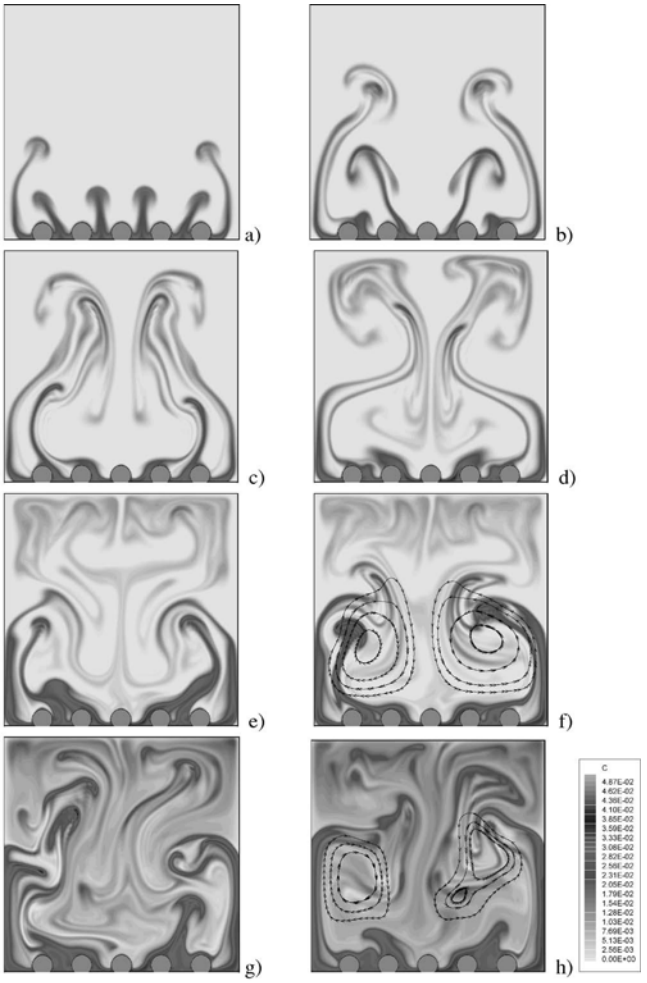

FIG. 7. Computed pattern formation and evolution for the case $N=5$, with $\partial T/\partial x=2\ ^\circ\mathrm{C\ cm^{-1}}$ ($T_{\mathrm{bottom}}=23\ ^\circ\mathrm{C}$, $T_{\mathrm{Top}}=29\ ^\circ\mathrm{C}$), subsequent snapshots corresponding to (a) $t=26.9$ s, (b) $t=32.9$ s, (c) $t=38.9$ s, (d) $t=48.3$ s, (e) $t=55.8$ s, (f) $t=58.9$ s, (g) $t=82.7$ s, (h) $t=91.8$ s.

$\cong 30$ s [see Fig. 7(b)], the plumes 1 and 2, and 5 and 6 merge so that the lighter fluid is transported upward by four solutal rising jets only. The surviving solutal plumes are located approximately above the first two drops (1 and 2) and the last two ones (4 and 5), whereas pluming phenomena at $y=L/2$ are prevented. For $t>40$ s, further coalescence of adjacent plumes occurs and a new regime arises with only two lateral rising main convective structures and a return fluid current descending from the top of the container toward the central drop at $y=L/2$; correspondingly, the space above the droplets is characterized by the presence of two counter-rotating vortices; see, e.g., Figs. 7(f) and 7(h). This regime is strongly oscillatory since the lateral fingers are periodically fed with new "packets" of solute.

Some preliminary conclusions can be drawn on the basis of these simulations: for both cases $N=4$ and $N=5$; unlike the final erratic pulsations observed for isothermal conditions, the system undergoes a transition to quite regular pattern oscillations with well-defined flow structures above the droplets.

C. Periodic boundary conditions

In this section, the results with no-slip lateral walls treated in Sec. IV B are compared with corresponding simulations obtained assuming periodic conditions (hereafter referred to as PBC) at the lateral boundaries. This case is considered to indirectly assess the role played by lateral geometrical constraints in determining edge effects and the pattern selection process. Also, such results provide a variety of interesting insights into the "extreme" behavior, which the system tends to, when the number of interacting droplets is increased to infinite ($N\rightarrow\infty$) at fixed values of the interspace parameter κ (i.e., infinite layer of liquid with evenly spaced droplets on the bottom).

As a first step, comparison between the computations for $\kappa=0.33$ and $N=4$ (PBC, shown in Fig. 8) and those with solid walls (SW), and same value of κ (Fig. 6) highlights that in the absence of side solid constraints, the delicate evolutionary equilibrium of the velocity field is featured by a different time history [compare, e.g., Fig. 8(a) with Fig. 6(b) and Fig. 8(b) with Fig. 6(c)]. Therefore, as expected, the

TABLE II. Computed oscillatory regimes in nonisothermal conditions ($\partial T/\partial x = 2\ ^\circ\mathrm{C\ cm^{-1}}$) and related frequencies as a function of N and of the boundary conditions type.

N	Boundary conditions	Regime	f (Hz)
4	SW	Single oscillatory standing vortex	2.63×10^{-2}
5	SW	Two oscillatory standing vortices	4.34×10^{-2}
4	PBC	Traveling wave	5.43×10^{-2}
5	PBC	Traveling wave	3.52×10^{-2}

absence of lateral solid constraints can be thought of as altering in a significant way the mode selection process and the pattern symmetries.

The major outcome of these studies (specially conceived to allow for lateral freedom], however, is that the final oscillatory state [already depicted in detail in Sec. IV B for the SW cases with a well-defined "standing" single cell or a well-defined "standing" couple of vortices above the droplets for $N=4$ and $N=5$, respectively), is replaced for PBC by the occurrence of a "traveling wave" migrating along the horizontal direction. This behavior is clearly shown in Fig. 9 for the case $N=4\rightarrow\kappa=0.33$ (the phenomena for $N=5\rightarrow\kappa=0.4$ are qualitatively similar to that for $\kappa=0.33$; therefore they are not discussed in detail).

The evolutionary scenario is driven by the continuous propagation along y of the position, where the shooting of the "packet" of lighter fluid in the surrounding liquid occurs. In other words, the front of the aforementioned wave corresponds at any time to the onset of a new rising plume. For instance, in Fig. 9(a) the main rising plume is originated from the space between droplets 1 and 2 whereas in Figs. 9(c), 9(e), and 9(g) such a position has moved to the interspace between droplets 2 and 3, 3 and 4, and 4 and 1, respectively. This also means that the spectrum of possible plume phase shifts is not discrete but "continuous" along the horizontal direction y, i.e., $\Delta\varphi(y_1-y_2)=(y_1-y_2)/\varpi$, ϖ being the wave propagation velocity ($\varpi=f\cdot L$, f being the frequency given in Table II). Owing to the combined presence of a disturbance traveling toward the top (i.e., a perturbation of the solutal and flow field rising at a given position y) and the simultaneous propagation of the related onset along the horizontal extension, the traveling wave can be regarded as a superposition of two perpendicular components (along y and x, respectively). Such a feature is also evidenced by the initial oblique inclination of the newly formed plumes.

Additional simulations carried out for isothermal conditions have revealed that in the absence of the Marangoni effect, such waves do not occur, even if PBC are employed. This proves that their origin is not of a pure gravitational type. Therefore, they do not have a solid kinship with the traveling states that have been occasionally reported in the literature in the case of thermosolutal convection in fluid layers of a wide horizontal extent[15,16] (see later).

Deane *et al.*[15] revealed, by means of two-dimensional

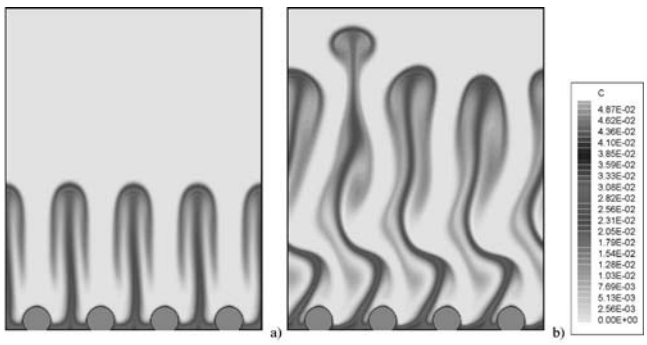

FIG. 8. Computed traveling wave for the case $N=4$ with PBC for the same thermal conditions corresponding to Fig. 6, subsequent snapshots: (a) $t=35.56$ s, (b) $t=47.53$ s.

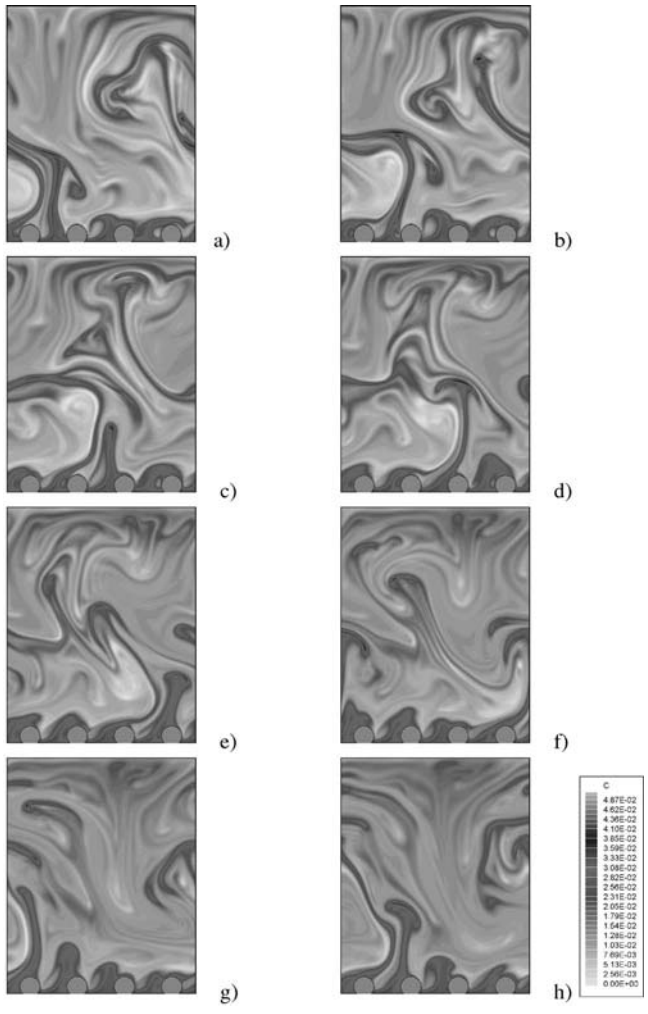

FIG. 9. Computed traveling wave for the case $N=4$ with PBC for the same thermal conditions corresponding to Fig. 6, subsequent snapshots: (a) $t=79.9$ s, (b) $t=82.3$ s, (c) $t=84.8$ s, (d) $t=87.5$ s, (e) $t=90.1$ s, (f) $t=92.8$ s, (g) $t=95.5$ s, (h) $t=98.3$ s (the period is 18.4 s).

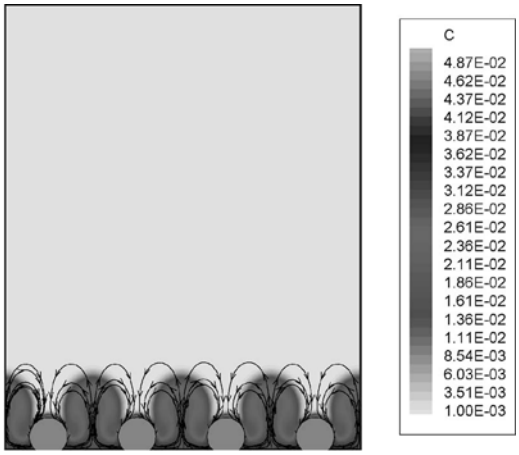

FIG. 10. Concentration and velocity fields for the case $N=4$ with PBC for the same thermal conditions corresponding to Fig. 6 under zero-g conditions (buoyancy absent), $t=85.32$ s.

numerical simulations of thermosolutal gravitational convection, the presence of oscillations in the form of traveling, standing, modulated, and chaotic waves. Similarly, Walden *et al.*[16] during studies of Rayleigh-Bénard convection in binary alcohol-water mixtures, observed the convective rolls to move continuously as traveling waves with either a periodic or chaotic nature according to the temperature difference across the fluid layer (i.e., the Rayleigh number, Ra).

As a subsequent natural step to investigate the intrinsic nature of the present waves, some computations have been repeated "uncoupling" the temperature field (i.e., assuming a fixed linear temperature distribution along y with the same temperature gradient considered for the results in Fig. 9). Such an artifice has shown that the presence of "static" Marangoni forces is not sufficient to explain the presence of the waves (they are suppressed). In practice, these results can be regarded as indirect evidence of the fact that the dynamical interplay among solutal buoyancy and thermal surface tension forces and/or the dynamical interaction among velocity, solutal and temperature fields are a necessary requisite for the onset of this type of instability. This conclusion is also supported by the numerical simulations carried out for the case of gravitational effects switched off and droplets subjected to the action of Marangoni forces alone. The simulations show that in the absence of gravity, unlike buoyancy convection, Marangoni convection originated from a multidroplet configuration does not affect the entire enclosure. Rather, the flow is restricted to an area close to the drop surfaces (see Fig. 10). Continuity brings the hot fluid (carried from the peak of the drop into the lower regions of the domain just below the drop base) up again, resulting in a set of closed vortices. Above this region, convection is very weak and the solute is simply transported by diffusion. Accordingly no solutal fingers exist, and the rich variety of scenarios with interacting plumes occurring under the effect of gravity is suppressed.

V. COMPARISON WITH OTHER RESULTS: ERRATIC PULSATIONS AND KICKING PHENOMENA

It is worthwhile to stress how the behaviors discussed previously are heretofore unseen and represent a new contribution to the fluid dynamics of drops in liquid-liquid systems (fundamental research) as well as to the field of materials (with miscibility gap) science.

It is interesting to point out, however, that these oscillatory behaviors exhibit some remarkable analogies with other systems in nature and/or with other results in the literature.

For instance, recent excellent experimental studies have pointed out that surfactants can also play a crucial role in creating interfacial instabilities in binary liquid-liquid systems and oscillation (referred to as "kicking" by these authors) of drops (see, e.g., Perez de Ortiz and Sawistowski,[13] Liang and Slater,[17] and Bekki *et al.*[18,19]).

The effect of surfactants on interfacial mass transfer in binary liquid-liquid systems (dissolving drops) was experimentally investigated by Agble and Mendes Tatsis[20] using the schlieren and the Mach-Zehnder optical techniques. The experiments were focused on the analysis of interfacial stability by means of direct examination of the interface of a drop of an organic phase (saturated with water) which was immersed in an aqueous phase of pure water. The onset of Marangoni convection and of possible fluid-dynamic instabilities at the interface was clearly observed. The role played by the surfactants (these substance can alter the surface tension) in inducing possible surface instabilities was investigated in detail in a subsequent analysis (Agble and Mendes Tatsis[21]). In this excellent analysis much room was devoted to compare the available experimental results with canonical and/or semiempirical surface stability criteria introduced over the years for the case of various binary liquid-liquid interfaces in the presence of a transferring surfactant; i.e., the Sternling and Scriven[22] criteria for ternary systems, the excellent Hennenberg *et al.*[23,24] criteria for surfactant transfer, the semiempirical criteria of Nakache *et al.*[25] It was found that these criteria often fail in predicting the observed phenomena. Along these lines, it is our opinion that many of the phenomena mentioned previously in the case of added surfactants could be explained according to the results discussed in Secs. IV B and IV C, the thermal surface tension gradient being simply replaced by the effect of the concentration gradient of surfactant for the cases above. Experimental conditions somewhat more similar to those considered in the present article were investigated by Zander *et al.*,[26] who studied the liquid-liquid phase decomposition induced in a horizontal fluid layer being exposed to a vertical temperature gradient. They reported the existence of some convective instabilities in the form of "dissipative structures" (regular convective patterns) inside the layer that indirectly manifested themselves by the organization of the floating precipitate. Some attempts were given to explain the appearance of these instabilities according to the model of a two-component Rayleigh-Bènard instability (also see the focused discussion in Sec. VI) driven by the temperature and concentration differences between the lower and the upper boundaries of the fluid (the concentration difference resulting from

the dependence of the local equilibrium composition on the local temperature). Such a criterion, however, was found not to properly model the experimental results; this was attributed to the influence of the Marangoni driven flows near the deposited droplets.

In the light of the present results, the "dissipative structures" indirectly observed by Zander *et al.*,[26] might be due to the indirect effect of the standing convective structures described in Sec. IV B.

The present simulations could also shed some light on other similar phenomena that have been observed, even in the absence of surfactants and imposed thermal gradients. For instance, many authors (see, e.g., the pioneering analysis of Lewis and Pratt[27]) observed rippling and erratic pulsations at the interface of drops of organic solvents dispersed in various solvents. According to Sec. IV A, they could be explained on the basis of the pure buoyant oscillatory instability that can occur (even in the absence of Marangoni effects) when many close droplets "interact."

VI. COMPARISON WITH OTHER MULTIPLUME CONFIGURATIONS: ANALOGIES AND DIFFERENCES

For the present case [$\mathrm{Ra}=O(10^8)$], all the solutal plumes shown in Figs. 3, 4, 6, and 7, etc., exhibit during the early stages of evolution a clear and distinct shape with a thin stem and a well-defined head with side lobes. As each plume rises, before coalescence with other plumes occurs, it widens as a natural consequence of diffusion of both solute and momentum, but the plume lobes tend to remain relatively distinct (this corresponds to the "viscous-nondiffusive" plume regime delineated by Hier Majumder *et al.*[28]). The literature about single-plume cases and related instabilities (the buoyant plume/jets of gas mixtures, pool fires, etc.) has been summarized in Lappa *et al.*[6] This section is devoted to a comparison with other multiplume systems available in the literature.

It is noteworthy how, from a fluid-dynamic point of view, that the problem under investigation exhibits quite an interesting theoretical kinship with the classical Rayleigh-Bènard (RB) system in which convection is induced in a fluid by uniform heating from below. Therefore, it is opportune to open a short discussion about the related analogies and differences. Such a critical comparison is used as an additional theoretical artifice by which additional insights into the physics and the results described in the earlier sections can be obtained.

Thermal Rayleigh-Bènard convection is a canonical example of a pattern forming system. A fascinating question is raised by the pattern selection process upon which it evolves through time to a final state. The number of rising plumes (also referred to as "wavenumber" in many circumstances) selection has been well studied, with many different mechanisms now well characterized.

Most of the initial studies considered infinite systems, i.e., the stability of the quiescent state of nonconfined fluid layers heated from below. Currently, however, it is well known that if systems confined laterally by rigid sidewalls are considered, even in containers of large horizontal dimensions, the lateral walls can have a significant influence on the flow pattern that develops when the Rayleigh number exceeds its critical value (for a given Ra, the wavelength basically depends on the aspect ratio of the container). The flow structure, however, becomes very complex when turbulent states are reached (very high values of the Rayleigh number).[29–34] It is known that the flow tends to develop into time-dependent convection with a strong asymmetry and highly convoluted thermal plumes delineating a large-scale circulation. In such conditions smaller thermal plumes can detach from thermal boundary layers and extend over the entire cell, coalescing and creating a local inversion of the temperature gradient adjacent to the boundary layers (see, in particular, Werne[35] and Vincent and Yuen[36]).

According to the aforementioned "analogy," these features may provide a somewhat relevant theoretical background to explain the trends observed for the present case of square domain with dissolving droplets on the bottom; among them: the time-dependent plume release and adjustment process and the related coalescence phenomena.

It should also be mentioned that possible analogies are not limited to RB systems; the present problem, in fact, also exhibits quite an interesting theoretical link with the Rayleigh-Taylor (RT) instability. Within the present context, it is worth considering for comparison/discussion the work of Bizon *et al.*[37]

They considered turbulent convection driven by an imposed concentration gradient in an isothermal vertical thin square Hele-Shaw cell ($24\ \mathrm{cm}\times 24\ \mathrm{cm}\times 0.1\ \mathrm{cm}$) at very high Rayleigh numbers (up to 7×10^4 times the value for convective onset). The vertical density gradient was, in practice, imposed by these researchers using a heavy fluid at the top horizontal boundary and a light fluid (like in the present work) at the bottom (both imposed fluids being solutions of iodine in ethyl alcohol).

They found the concentration field at such high values of the Rayleigh number to be characterized by sharp concentration gradients at the top and bottom boundaries (the concentration gradients corresponding to the presence of boundary layers) and a central core region with mean concentration not dependent on height; the velocity field was shown to be featured by the release of solutal plumes growing up the aforementioned boundary layers (the large density difference between the boundary fluid and the central core driving a Rayleigh-Taylor instability responsible for plume formation).

They observed that the previously mentioned instability of the boundary layer tends to excite the formation of many, closely spaced plumes whose number always exceeds that predicted in the case of simple RB convection. They also reported coalescence of these boundary-layer plumes resulting from (1) sweeping motions caused when fluid moving from the interior strikes the boundary and then spreads out horizontally, and/or (2) mutual interactions between neighboring plumes already known in the case of canonical thermal RB.[38]

Conglomerates of plumes leaving the boundary were observed to form "conduits" that organize the vertical transport and "channel" subsequent plumes (the channeled fluid, upon impacting and spreading along the far boundary, provides the

sweeping motion that organizes the boundary-layer plumes there into return vertical channels).

Despite the macroscopic qualitative similarities with turbulent RB and RT systems, however, the dynamics and the mechanisms underlying the evolution of the present system are quite different.

In the case of RB and RT configurations, the driving force for the onset of convection is the lighter fluid on the bottom of the container, this "force" being replaced by the presence of a discrete distribution of sources of solute for the case of a discrete distribution of droplets. However, there is no doubt that the geometries that arise in immiscible alloys processing, are more complicated than a simple classical RB or RT system. For such a case the distribution of light fluid at the bottom is not uniform. The light solute-enriched zones do not exhibit uniform behavior. Moreover, during the initial stages of convection fluid motion also arises along the lateral boundaries of the droplets (this effect is not present in the classical Rayleigh-Bènard system; within the framework of the proposed analogy, it would correspond to a "heating-from-the-side" thermal condition).

For many interacting droplets, the adjustment in the number of plumes involves the overlapping mechanisms of the enriched zones that merge as time passes; there is an undeniable effect of the number of droplets and their distribution.

Therefore, for the case of many aligned evenly spaced dissolving droplets, after the early stages (with an alternating array of clockwise and counterclockwise rotating cells), the process by which the instantaneous mode is selected is very complicated (possibly involving the effects of multiple incommensurate selection mechanisms). There are at least five independent parameters influencing the aforementioned evolution of the multicellular and multiplume structure, i.e., the aspect ratio of the container and/or the type of lateral boundary conditions, the time-evolution of the phenomenon of release of solute (this would correspond to a quasisteady variation of the Rayleigh number for the case of the layer of fluid heated from below), the coalescence process of the enriched zones originated from different drops, the number of interacting droplets (as previously highlighted), and finally the possible presence of surface Marangoni effects.

In practice, such a system would "ideally" tend to the behavior of the classical infinite RB or RT problem only if PBC conditions and a zero separation distance among the droplets (i.e., a uniform horizontal layer of liquid formed by the coalescence process of very close droplets) were considered.

Many investigations have also appeared in the literature for the case of multiple localized sources of buoyancy (instead of uniform conditions at the bottom). To the author's knowledge, however, these studies have been focused on flows of different types, but all dealing with large-scale scenarios, e.g., geological flows (Farnetani *et al.*[39]) or environmental problems and (see, e.g., Lavelle[40] and the rich reference list therein). Hydrothermal plumes originated from the deep-sea floor are one of many examples in the natural environment where a localized source of buoyancy causes materials to rise into an overlying fluid and forced circulation to develop. Plumes from terrestrial volcanoes, forest fires, urban mass fires, and oceanic thermal and waste water discharges (e.g., jet groups issuing from ocean outfalls) provide instances of buoyant plumes or buoyant jets occurring in a cross-flow. A related problem in the industrial realm involves the dispersion of power plant plumes into the atmosphere and associated chemical reactions, interaction and spreading of cooling tower plumes, burning of oil spills on water, etc.

Studies about smoke dispersion from multiple fire plumes have shown that multiple-plume interactions can push particulate up to altitudes exceeding that of an equivalent single plume (Trelles *et al.*[41]). These interactions can have unexpected results on the containment of airborne material. The mixing promoted by the large-scale plume vortex structures can transport combustion products to areas that would not have been covered by a single plume produced by a single fire.

The investigation of König and Mokhtarzadeh-Dehghan[42] was aimed to verify the question of how closely the overall characteristics of merged plumes from a multiflue chimney match those of an equivalent single plume. The results for multiflue plumes were compared with those for a single plume under the same release conditions for volume flow rate, momentum, and temperature. The differences in the velocity, temperature, and turbulence energy fields of a single plume and multiple plumes were found to be mainly significant in the early stages of rise and spreading.

Bornoff and Mokhtarzadeh-Dehghan[43] presented the results of a numerical investigation into the interaction of two adjacent plumes in a cross-flow. The computations were performed for three-dimensional, turbulent, buoyant and interacting plumes, and for a single plume for comparison. Two double-source arrangements, namely, tandem and side-by-side with respect to the oncoming atmospheric boundary layer, were considered. The results showed that the interaction of side-by-side plumes is dominated by the interaction of the rotating vortex pairs within the plumes. A tandem source arrangement leads to early merging and efficient rise enhancement.

Davies *et al.*[44] carried out experiments to measure concentration fluctuations downwind of two tracer sources in the atmospheric surface layer. They showed that the correlation between the concentrations from the two sources varies with downwind distance and source separation. These studies about nonconfined flows (free plumes) and the emission and dispersion of pollutants or the rise of oceanic or geophysical currents, though very interesting, however, are not very relevant to the present case of interacting plumes in a closed geometry, and direct comparison is very difficult or impossible. They have been cited here for the sake of completeness and are of little help when trying to get additional insights into the physics of the problem treated in this work.

VII. CRITICAL DISCUSSION AND CONCLUSIONS

The different complex scenarios that arise in a container filled with an organic binary system in nonequilibrium conditions (accommodating many droplets on the bottom) in terms of a detailed structure of the convective field and pat-

tern of the concentration field, have been investigated for the first time by means of solution of the nonlinear model (Navier-Stokes) equations. A multiphase methodology has been used to address the geometric complexity introduced by the internal droplets.

The simulations have proven that, even in the absence of Marangoni effects, time-dependent "pulsating" phenomena can occur if a multidroplet configuration is considered. In such a case, in fact, the generation of jets results modulated in time with an intriguing temporal alternation of buoyant plumes originated from different locations within the container.

After a short initial transient time in which the system exhibits mirror symmetry with respect to the midsection, progression from order to disorder occurs and the system undergoes transition to a condition in which the time-dependent release of solutal plumes becomes erratic from both spatial and temporal points of view.

If a temperature gradient is applied to the system, the evolutionary progress is different. It is known that in such conditions, even for isolated droplets, the onset of oscillatory instabilities is possible according to the interplay between buoyancy and Marangoni effects. However, for $N>1$ the time-dependent dynamics of the considered system is significantly influenced by the fact that the presence of descending currents along the surface of the drops (induced by the surface tension forces) changes the number and the position of the rising solutal jets with respect to isothermal conditions.

Due to the Marangoni surface descending currents, the plumes are originated from the middle space between consecutive droplets rather than from their surface. Also, for the same reason, the number of rising plumes generated by a given number of interacting droplets is larger in the case of non-isothermal conditions. Such a feature, owing to the delicate interplay among a larger number of plumes, affects the possible transitional states of the multidroplet system. Moreover, the final flow spatio-temporal organization with a single vortex above the droplets in the case $N=4$ and two mirror (approximately) vortices for $N=5$ tends to be more regular than the final erratic behavior occurring in the absence of Marangoni effects; in other words the presence of thermal surface tension effects favors the establishment of coherent repetitive structures from a global point of view. Such "standing" convective phenomena, however, are replaced by the propagation of traveling waves along the horizontal extension of the domain when periodic conditions are assumed at the side boundaries.

In terms of possible plume time shifts, the aforementioned phenomena can be categorized as follows: chaotic (lateral SW and isothermal conditions), discrete (lateral SW and non isothermal conditions) and continuous (lateral PBC and non isothermal conditions) phase-shifts distributions, respectively. In terms of macroscopic features of the unsteady evolution, a corresponding categorization would read: erratic pulsation, standing pulsation, and traveling pulsation, respectively.

The results are heretofore unseen and elucidate how the simultaneous presence of several dispersed droplets in non-equilibrium conditions can be responsible for the onset of a variety of additional instabilities with respect to the case of an isolated drop (that make such a configuration a pattern-forming dynamical system of exceptional complexity). It exhibits sensitivity to the number of droplets and, in turn, each droplet and the related surrounding convective structure undergo different evolution according to the position within the container.

This study represents an attempt to discern the cause and effect relationships underlying the complexity related to the processing on the ground of immiscible metal or organic alloys. Also, it may explain some still controversial results in the literature dealing with the observation of pulsating ("kicking") behaviors during the phase separation process of transparent liquid-liquid systems with a miscibility gap. A comparison with convection in other canonical systems has been considered. Other interesting phenomena dealing with the processing of these types of materials and the dynamics of dispersed droplets are treated in companion works.[45,46]

ACKNOWLEDGMENT

The author would like to thank Dr. C. Piccolo (MARS) for providing Fig. 5.

[1] L. Ratke, "Decomposition, phase separation, solidification of immiscible liquid alloys," in *Immiscible Liquid Metals and Organics*, Proceedings of an International Workshop Organized by the ESA Expert Working Group, "Immiscible alloys" held in the Physikzentrum, Bad Honnef 1992, edited by L. Ratke (Informationsgesellschaft, Germany, 1992), pp. 3–34.
[2] M. Wu, A. Ludwig, and L. Ratke, "Modelling the solidification of hypermonotectic alloys," Modell. Simul. Mater. Sci. Eng. **11**, 755 (2003).
[3] E. Bassano, "Numerical simulation of thermo-solutal-capillary migration of a dissolving drop in a cavity," Int. J. Numer. Methods Fluids **41**, 765 (2003).
[4] M. Lappa, "Assessment of VOF strategies for the analysis of Marangoni migration, collisional coagulation of droplets and thermal wake effects in metal alloys under microgravity conditions," Computers, Materials and Continua **2**, 51 (2005).
[5] A. Esmaeeli, "Phase distribution of bubbly flows under terrestrial and microgravity conditions," Fluid Dynamics and Materials Processing **1**, 63 (2005).
[6] M. Lappa, C. Piccolo, and L. Carotenuto, "Mixed buoyant-Marangoni convection due to dissolution of a droplet in a liquid-liquid system with miscibility gap," Eur. J. Mech. B/Fluids **23**, 781 (2004).
[7] M. Lappa, C. Piccolo, L. Carotenuto, and R. Savino, "Fluid-dynamics and dissolution kinetics in immiscible organic systems with dispersed droplets," Colloids Surf., A **261**, 177 (2005).
[8] M. Lappa and C. Piccolo, "Higher modes of mixed Buoyant-Marangoni unstable convection originated from a droplet dissolving in a liquid/liquid system with miscibility gap," Phys. Fluids **16**, 4262 (2004).
[9] M. Kassemi and N. Rashidnia, "Steady and oscillatory thermocapillary convection generated by a bubble," Phys. Fluids **12**, 3133 (2000).
[10] M. Lappa, "Growth and mutual interference of protein seeds under reduced gravity conditions," Phys. Fluids **15**, 1046 (2003).
[11] G. Amberg and J. Shiomi, "Thermocapillary flow and phase change in some widespread materials processes," Fluid Dynamics and Materials Processing **1**, 81 (2005).
[12] M. Lappa, "Numerical strategies for the simulation of dissolution kinetics and fluid-dynamic instabilities in liquid couples with a miscibility gap," J. Non-Equilib. Thermodyn. **30**, 243 (2005).
[13] E. Susana Perez de Ortiz and H. Sawistoski, "Interfacial instability of binary liquid-liquid systems, I. Stability analysis," Chem. Eng. Sci. **28**, 2051 (1973).
[14] M. Lappa, "Strategies for parallelizing the three-dimensional Navier-Stokes equations on the Cray T3E," Science and Supercomputing at CINECA **11**, 326 (1997).
[15] A. E. Deane, E. Knobloch, and J. Toomre, "Traveling waves and chaos in thermosolutal convection," Phys. Rev. A **36**, 2862 (1987).
[16] R. W. Walden, P. Kolodner, A. Passner, and C. M. Surko, "Traveling

waves and chaos in convection in binary fluid mixtures," Phys. Rev. Lett. **55**, 496 (1985).
[17]T. B. Liang and M. J. Slater, "Liquid-liquid extraction drop formation: mass transfer and the influence of surfactant," Chem. Eng. Sci. **45**, 97 (1990).
[18]S. Bekki, M. Vignes-Adler, E. Nakache, and P. M. Adler, "Solutal Marangoni effect: I. Pure interfacial transfer," J. Colloid Interface Sci. **140**, 492 (1990).
[19]S. Bekki, M. Vignes-Adler, and E. Nakache, "Solutal Marangoni effect: II. Dissolution," J. Colloid Interface Sci. **152**, 314 (1992).
[20]D. Agble and M. A. Mendes-Tatsis, "The effect of surfactants on interfacial mass transfer in binary liquid-liquid systems," Int. J. Heat Mass Transfer **43**, 1025 (2000).
[21]D. Agble and M. A. Mendes-Tatsis, "The prediction of Marangoni convection in binary liquid-liquid systems with added surfactants," Int. J. Heat Mass Transfer **44**, 1439 (2001).
[22]C. V. Sternling and L. E. Scriven, "Interfacial turbulence: Hydrodynamic instability and the Marangoni effect," AIChE J. **5**, 514 (1959).
[23]M. Hennenberg, P. M. Bisch, M. Vignes-Adler, and A. Sanfeld, "Mass transfer Marangoni and instability of interfacial longitudinal waves I. Diffusional exchanges," J. Colloid Interface Sci. **69**, 128 (1979).
[24]M. Hennenberg, P. M. Bisch, M. Vignes-Adler, and A. Sanfeld, "Mass transfer Marangoni and instability of interfacial longitudinal waves II. Diffusional exchanges and adsorption-desorption processes," J. Colloid Interface Sci. **74**, 495 (1979).
[25]E. Nakache, M. Dupeyrat, and M. Vignes-Adler, "Experimental and theoretical study of an interfacial instability at some oil-water interfaces involving a surface-active agent: I. Physicochemical description and outlines for a theoretical approach," J. Colloid Interface Sci. **94**, 120 (1983).
[26]R. Zander, M. Dittman, and G. M. Schneider, "Dissipative structures in demixing binary liquid systems," Z. Naturforsch., A: Phys. Sci. **45**, 1309 (1990).
[27]J. B. Lewis and H. R. C. Pratt, "Oscillating droplets," Nature (London) **171**, 1155 (1953).
[28]C. A. Hier Majumder, D. A. Yuen, and A. Vincent, "Four dynamical regimes for a starting plume model," Phys. Fluids **16**, 1516 (2004).
[29]B. R. Taylor, G. Taylor, and J. S. Turner, "Turbulent gravitational convection from maintained and instantaneous sources," Proc. R. Soc. London, Ser. A **234**, 1 (1956).
[30]J. S. Turner, "Buoyant plumes and thermals," Annu. Rev. Fluid Mech. **1**, 29 (1969).
[31]T. Y. Chu and R. J. Goldstein, "Turbulent convection in a horizontal layer of water," J. Fluid Mech. **60**, 141 (1973).
[32]B. Castaing, G. Gunaratne, F. Heslot, L. Kadanoff, A. Libchaber, S. Thomae, X. Wu, S. Zaleski, and G. Zanetti, "Scaling of hard thermal turbulence in Rayleigh-Bènard convection," J. Fluid Mech. **204**, 1 (1989).
[33]T. H. Solomon and J. P. Gollub, "Sheared boundary layers in turbulent Rayleigh-Bènard convection," Phys. Rev. Lett. **64**, 2382 (1990).
[34]E. Siggia, "High Rayleigh number convection," Annu. Rev. Fluid Mech. **26**, 137 (1994).
[35]J. Werne, "Structure of hard-turbulent convection in two dimensions: Numerical evidence," Phys. Rev. E **48**, 1020 (1993).
[36]A. P. Vincent and D. A. Yuen, "Plumes and waves in two-dimensional turbulent thermal convection," Phys. Rev. E **60**, 2957 (1999).
[37]C. Bizon, J. Werne, A. A. Predtechensky, K. Julien, W. D. McCormick, J. B. Swift, and H. L. Swinney, "Plume dynamics in quasi-2D turbulent convection," Chaos **7**, 107 (1997).
[38]E. Moses, G. Zocchi, I. Procaccia, and A. Libchaber, "The dynamics and interaction of laminar thermal plumes," Europhys. Lett. **14**, 55 (1991).
[39]C. Farnetani, B. Legras, and P. Tackley, "Mixing and deformations in mantle plumes," Earth Planet. Sci. Lett. **196**, 1 (2002).
[40]J. W. Lavelle, "Buoyancy-driven plumes in rotating, stratified cross flows: Plume dependence on rotation, turbulent mixing, and cross-flow strength," J. Geophys. Res. **102**, 3405 (1997).
[41]J. Trelles, K. B. McGrattan, and H. R. Baum, "Smoke dispersion from multiple fire plumes," AIAA J. **37**, 1588 (1999).
[42]C. S. König and M. R. Mokhtarzadeh-Dehghan, "Numerical study of buoyant plumes from a multiflue chimney released into an atmospheric boundary layer," Atmos. Environ. **36**, 3951 (2002).
[43]R. B. Bornoff and M. R. Mokhtarzadeh-Dehghan, "A numerical study of interacting buoyant cooling-tower plumes," Atmos. Environ. **35**, 589 (2001).
[44]B. M. Davies, C. D. Jones, A. J. Manning, and D. J. Thomson, "Field experiments on the interaction of plumes from two sources," Q. J. R. Meteorol. Soc. **126**, 1343 (2000).
[45]M. Lappa, "Coalescence and non-coalescence phenomena in multimaterial problems and dispersed multiphase flows: Part 1, a critical review of theories," Fluid Dynamics and Materials Processing **1**, 201 (2005).
[46]M. Lappa, "Coalescence and non-coalescence phenomena in multimaterial problems and dispersed multiphase flows: Part 2, a critical review of CFD approaches," Fluid Dynamics and Materials Processing **1**, 213 (2005).